

Feedback induced phase transitions in active porous media

Samuel A. Ocko¹ and L. Mahadevan²

¹*Department of Physics, Massachusetts Institute of Technology, Cambridge, Massachusetts 02139, USA*

²*School of Engineering and Applied Sciences, Department of Physics, Harvard University, Cambridge, Massachusetts 02138, USA*

(Dated: September 13, 2021)

Flow through passive porous media is typically described in terms of a linear theory relating current fluxes and driving forces, in the presence of a prescribed heterogeneous permeability. However, many porous systems such as glacial drainage networks, erosional river bed networks, vascular networks, social insect swarms and animal architectures such as termite mounds are continuously remodeled by the flow and thence modify the flow, i.e. they are active. Here we consider a minimal model for an active porous medium where flow and resistance are coupled to each other. Using numerical simulations, we show that this results in both channelization and wall-building transitions depending on the form of the feedback. A continuum model allows us to understand the qualitative features of the resulting phase diagram, and suggests ways to realize complex architectures using simple rules in engineered systems.

Introduction: Transport through porous media is important in many problems in physics, biology, geology, and engineering. While most study is limited to transport through a *static* medium, transport can often feedback to modify the medium itself. These *active* porous media co-evolve with the transport through them.

Examples of active porous media abound. River networks are formed through the interplay of erosion, transport, and deposition[1, 2], lightning results from the interplay of conduction and dielectric breakdown, and electrical fuses are engineered to break down above a critical current[3, 4]. All life exists in a world of gradients and physical flows, and biological systems often arrange matter through feedback mechanisms to control transport at the cellular[5–9], organismal[10–15], and societal[16–21] level. Specific examples of active porous media in biology include network formation of slime molds, formation and remodeling of vascular networks, and the mound and wax architectures of social insects.

Elements universal across these active porous media are conservation of flow, feedback from transport and stochasticity. In drainage networks, erosion increases with current while deposition decreases, while fuses are more likely to break in high current, and dielectric breakdown is enhanced by large currents and fields. In biology, ants have been observed to remove corpses from high-wind areas and place them in low-wind areas [20], while termites are known to respond to mound damage by building in response to air flows, humidity, and olfactory cues [18, 21]. A minimal distillation of the common elements in these different active porous media corresponds to a stochastically evolving network driven uniformly by fluxes and forces at the boundary due to pressure, voltage, or concentration gradients. Since problems involving steady state diffusion of heat, concentration gradients, or flow through a porous material are mathematically analogous to current flow through electrical circuits, we will use the language of circuit theory from now on.

Transport Laws: We focus on a translationally symmetric case with periodic boundary conditions and a uni-

form driving voltage in the vertical \hat{z} direction. The vertices are arranged in a square network, with the current between neighboring vertices given by

$$I_{ij} = \frac{1}{\Omega_{ij}} ([V_i - V_j] + g\hat{z} \cdot \hat{\mathbf{r}}_{ij}), \quad \sum_j I_{ij} = 0. \quad (1)$$

Each vertex i either contains a particle ($\rho_i = 1$) or is empty ($\rho_i = 0$), with the resistance between full vertices higher than the resistance between empty vertices; $\Omega_{ij} = 1 + \Delta\Omega(\rho_i + \rho_j)/2$.

Activity Rules: Particles are removed from their vertices at a *current-dependent* rate proportional to $r(v_i)$, where $v_i = \sqrt{1/2 \cdot \sum_j I_{ij}^2}$ is the current through the cell [22]. They are then added to an empty vertex with probability proportional to $a(v_j)$, leading to a simple algorithm for evolution of the medium[23]:

1. Remove a particle from filled vertex i randomly selected with probability proportional to $r(v_i)$.
2. Solve for the new current through the network.
3. Add the particle to an empty vertex j randomly selected with probability proportional to $a(v_j)$.
4. Solve for the new current through the network.

We emphasize that every step conserves particle number, but the movement of particles is nonlocal in that the distance between vertices i, j may be arbitrarily large [24]. Note that the system lacks detailed balance and thus we cannot write down a free energy functional associated with the dynamics (Fig. 2).

Since the addition and removal rates can either increase or decrease with local current in the active systems described earlier, we explore this range of possibilities in terms of two parameters α_R, α_A . For the removal process, we choose $r(v_i) = v_i^{-\alpha_R}$; at positive α_R , particles in high current will be less likely to be removed (current seeking), and vice versa. For the addition process, we choose $a(v_j) = v_j^{\alpha_A}$; at positive α_A , empty vertices with high current will likely be filled (current seeking) and vice versa.

For simplicity, we have chosen our functional forms such that in any circuit, $r(v_i) \propto g^{-\alpha_R}$, $a(v_j) \propto g^{\alpha_A}$. Because only the *ratios* of currents are important, we may set this system of equations to be dimensionless by making the substitutions: $\Omega_0 \rightarrow 1$, $\Delta\Omega \rightarrow \Delta\Omega/\Omega_0$, $g \rightarrow 1$. This gives four dimensionless parameters: $\Delta\Omega$, α_R , α_A , $\bar{\rho}$. We want the difference between filled and unfilled vertices to be large; here we choose $\Delta\Omega = 19$ such that the resistance between filled vertices is 20 times higher than empty vertices.

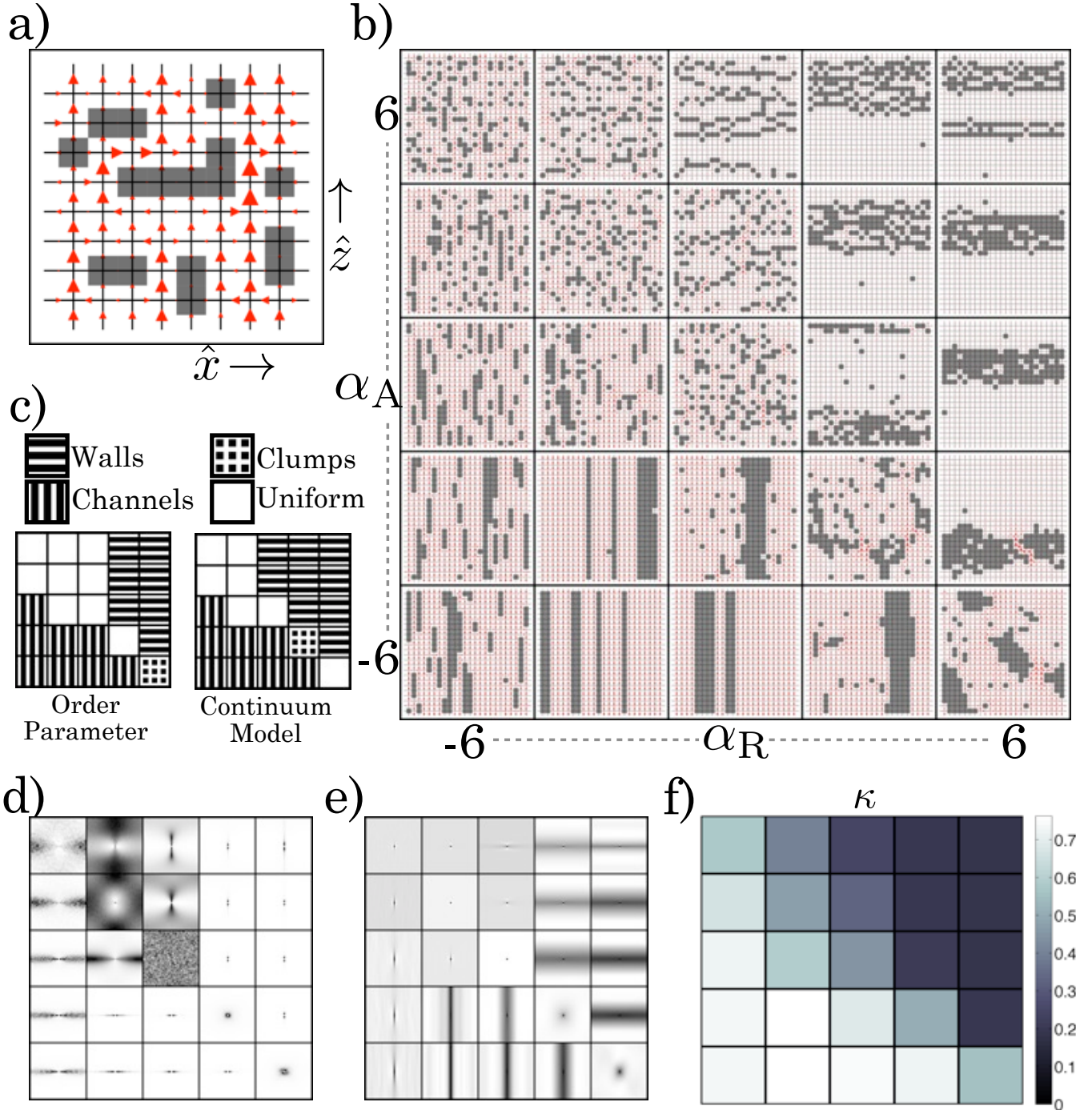


FIG. 1 a) Example system for $(\alpha_A, \alpha_R) = (0, 0)$. Filled vertices are covered by gray squares, unfilled vertices are not. Current is being driven in the upwards \hat{z} direction, direction and magnitude of current between neighboring vertices is indicated by red arrows(color online). b) Phase diagram for $\bar{\rho} = 1/4$. Each individual box represents a single system that has equilibrated for a particular (α_A, α_R) , where α_A, α_R have values $(-6, 3, 0, 3, 6)$. At positive α_R , the system has formed thick walls; negative α_R gives thin channels. At positive α_A , the system has formed a series of thin walls; negative α_A gives thick channels. At positive α_R , negative α_A , a phase separation occurs at both orientations, as the system forms a set of clumps. c) Observed phase transitions through observation of order parameters on ensemble(see text) vs. predictions of continuum model(see text). d) Fourier transform $\langle \bar{\rho}(\mathbf{k})^2 \rangle$ (high amplitudes in dark, $\mathbf{k} = 0$ at center). e) Two-point correlation $\langle (\rho(0) - \bar{\rho})(\rho(\vec{r}) - \bar{\rho}) \rangle$ (positive correlations in dark, $\mathbf{r} = 0$ at center). f) Contour plot of conductivity of the medium as a function of α_R, α_A . Note that grids c)-f) use the same range of α_A, α_R as grid b). Grids c)-f) use a system size of 40×40 , while grid b) uses a smaller system size of 24×24 to aid in visualization.

Simulations: For each α_R , α_A , $\bar{\rho}$, we start the system at a uniform density $\bar{\rho}$ and evolve it so that each particle or hole moves an average of one thousand times. This procedure is repeated twenty times for the parameters $\alpha_R, \alpha_A = (-6, -3, \dots, 3, 6)$, $\bar{\rho} = .25$., computing the current through the entire network at every step. The results in Fig. 1 show that the system spontaneously forms channels (with high conductivity) at sufficiently negative α_R, α_A , and spontaneously forms walls (with low conductivity) at sufficiently positive α_R, α_A . This kind of phase transition is similar to those seen in driven lattice gas models [25, 26].

When the system channelizes due to negative α_R , we find *thin* channels, with glassy behavior; a negative α_A gives *thick* channels. To understand these transitions, we consider their robustness to perturbations. When the system has formed a set of parallel channels, occasionally a channel gets blocked (Fig. 2 c). When the channel is thin, current must go through the clog blocking the channel, and therefore total current through the channel is reduced while the clogging particle has much of this current forced through it. On the other hand, when this channel is thick, current will go around the clog, and so is barely impeded. Therefore, at negative α_A , the thin channel has reduced current, and this clogging will cause the thin channel to fill, while a large channel is much more robust and will not be filled. On the other hand, for negative α_R , the clog in the wide channel has little current through it, and lingers, allowing the wide channel to eventually be filled; the clog in the thin channel has high current forced through it and is quickly removed. However, the system can become stuck in a glassy state-thick channels can form at negative α_R can persist, and multiple thick channels may persist at negative α_A . This can lead to large hysteretic effects which are especially strong at very negative α_A, α_R , when the system is “frozen” and fluctuations are suppressed.

For positive α_R , the system forms thick walls, while for positive α_A , the system forms a network of thin walls, although there does not appear to be a phase transition in this regime. In this state, occasionally a hole will form in the wall (Fig. 2 d). If the wall is thin, current rushes through the hole, and very little current goes through the rest of the wall. When the wall is thick, current through the wall and hole is roughly unchanged. Therefore, at positive α_R , the thin wall will quickly disintegrate as a result of the hole, while the thick wall will persist, and the hole will eventually get filled. On the other hand, at positive α_A , the hole in the thin wall will quickly be filled, while the hole in the thick wall will persist while more holes are allowed to appear. Interestingly, when α_R is positive and α_A is negative, both channelization *and* wall-building phase separations occur, as the system phase-separates into thick clumps. For some choices of parameters (positive α_A in Fig. 1) we see scale-free correlations, where the strength of a mode depends not on the magnitude of the wave-vector, but only its direction. As we will see, both these features follow from a continuum

model.

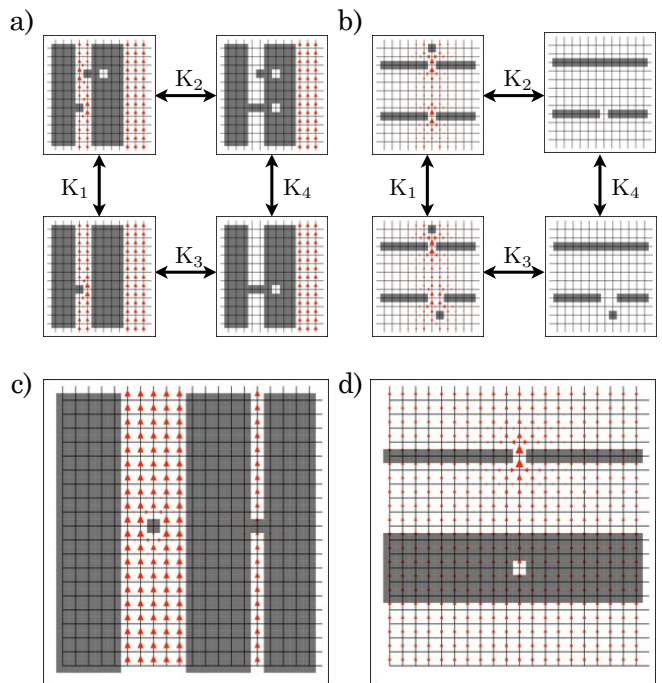


FIG. 2 a), b): Lack of detailed balance. In a), $\alpha_A < 0$, and $K_2 \approx K_3$, as the current through the lower right vertex has only weak dependence on the occupation of the upper left vertex. However $K_1 \not\approx K_4$, as the current through the upper left vertex strongly depends on the occupation of the lower right vertex; therefore $K_1 K_2 \neq K_3 K_4$. A similar proof follows for situation b), where $\alpha_A > 0$. c), d): Robustness of thick and thin structures (see text).

To characterize the wall-building phase separation, we use the row density $\rho_z = \sum_x \rho_{xz} / \mathbf{L}_x$ as an order parameter, consistent with the fact that when the distribution of row densities becomes bimodal (Fig. 3d example), wall-building has occurred. We characterize the channelization phase transition in terms of the column density $\rho_x = \sum_x \rho_{xz} / \mathbf{L}_z$; when this is bimodal, channelization has occurred (Fig. 1). We characterize a clumping phase transition through local density $\bar{\rho}_{\mathbf{r}} = 1/A \sum_{\mathbf{r}'} \theta(\sqrt{6} - |\mathbf{r} - \mathbf{r}'|) \rho_{\mathbf{r}'}$ where θ is the Heaviside function. [27]; when this is bimodal and neither column or row density are bimodal, clumping has occurred.

Continuum model: Characterizing the distribution of filled vertices with a mean density field ρ , the continuum version of Eq. 1 is:

$$\mathbf{J} = \kappa(\rho)(-\nabla V + g\hat{z}), \quad \nabla \cdot \mathbf{u} = 0 \quad (2)$$

where κ , the conductivity, is a function of density. Similarly, in the continuum limit, the discrete addition and removal activity are replaced with a stochastic equation

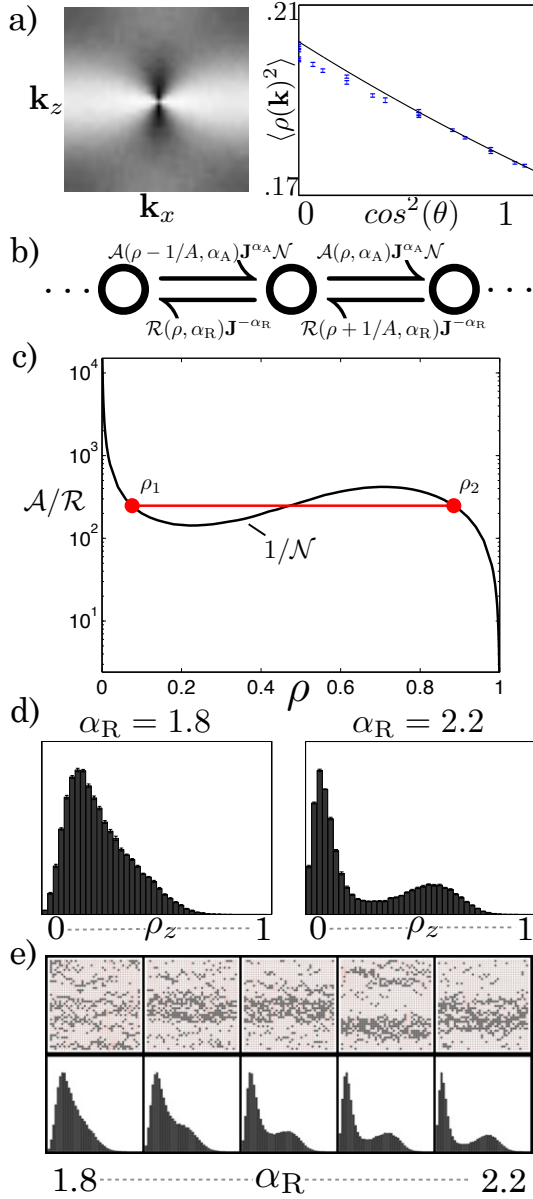


FIG. 3 a) $\langle \rho(\mathbf{k})^2 \rangle$ for $(\alpha_R, \alpha_A) = (.1, .1)$. Scatter plot of $\langle \rho(\mathbf{k})^2 \rangle$ vs. $(\hat{\mathbf{k}} \cdot \hat{x})^2 = \cos^2(\theta)$ for $(|\mathbf{k}|L)/2\pi \leq 5$ compared with prediction from continuum model. Note that the majority of dependence is on direction $\mathbf{k}_x^2/|\mathbf{k}^2|$, not magnitude $|\mathbf{k}|$. b) Fokker-Planck dynamics of continuum model for wall phase separation for a slice of area A . c) Visualization of Eqs. 4, 5, for $(\alpha_R, \alpha_A) = (2.6, 0)$ (color online) d) Comparison of histograms of row density, $\alpha_A = 0$ for a 40×40 system. The right histogram is bimodal, so a wall phase transition is considered to have occurred. e) Comparison of snapshots and row density histograms for wall-building phase transition.

for density evolution:

$$\dot{\rho} = -\mathcal{R}(\rho, \mathbf{J}, \alpha_R) + \mathcal{N}\mathcal{A}(\rho, \mathbf{J}, \alpha_A) + \eta \quad (3)$$

where $\mathcal{R}(\rho, \mathbf{J}, \alpha_R)$ is the mean removal rate from a region of with density ρ , a current of \mathbf{J} and a bias of α_R . \mathcal{A} is the mean addition rate, and \mathbf{J} is itself a functional of ρ obtained by solving Eq. 2. $\mathcal{N} = \iint \mathcal{R} / \iint \mathcal{A}$ acts as a sort of chemical potential, which is set to conserve total particle number. η is the stochastic noise term which creates fluctuations, whose form will be discussed later. [28]

The predictions of the continuum model depend strongly on the functions $\kappa, \mathcal{A}, \mathcal{R}$. To determine them, we use a *hybrid* approach, sampling via numerical experiment using randomly placed particles and then varying the density to approximate the entire functions, leaving us with no fitting parameters [29] As in the discrete case, we start with a uniform density of $\bar{\rho}$, $\mathbf{u}_0 = \kappa(\bar{\rho})$. [30]

Low α_R, α_A limit: In the limit where $\alpha_R, \alpha_A \rightarrow 0$, only the linear response is important. Writing Eq. 3 as

$$\dot{\rho} = -\mathcal{T}(\rho, \mathbf{J}, \vec{\alpha}) + \eta,$$

where $\mathcal{T}(\rho, \mathbf{J}, \vec{\alpha}) = -\mathcal{R}(\rho, \mathbf{J}, \alpha_R) + \mathcal{N}\mathcal{A}(\rho, \mathbf{J}, \alpha_A)$ is the time derivative functional, $\vec{\alpha} = (\alpha_R, \alpha_A)$, we note that :

$$\frac{d\mathcal{T}}{d\rho} = \left. \frac{\partial \mathcal{T}}{\partial \rho} \right|_{\mathbf{J}, \vec{\alpha}} + \left. \frac{\partial \mathcal{T}}{\partial \mathbf{J}_z} \right|_{\rho, \vec{\alpha}} \frac{\partial \mathbf{J}_z}{\partial \rho}.$$

Furthermore, we decompose density fluctuations into its Fourier basis:

$$\frac{d\mathcal{T}(\mathbf{k})}{d\rho(\mathbf{k})} = \left. \frac{\partial \mathcal{T}}{\partial \rho} \right|_{\mathbf{J}, \vec{\alpha}} + \left. \frac{\partial \mathcal{T}}{\partial \mathbf{J}_z} \right|_{\rho, \vec{\alpha}} \frac{\partial \kappa}{\partial \rho} \frac{\mathbf{k}_x^2}{|\mathbf{k}|^2},$$

where $\frac{\partial \mathbf{J}_z(\mathbf{k})}{\partial \rho(\mathbf{k})} = \frac{\partial \kappa}{\partial \rho} \frac{\mathbf{k}_x^2}{|\mathbf{k}|^2}$ (see Supplementary Information). Characterizing η as uncorrelated Gaussian noise via $\langle \eta(\mathbf{k}, t) \eta(\mathbf{k}', t') \rangle = 2\delta(t - t') \delta_{\mathbf{k} + \mathbf{k}'} D$, where $D = [\mathcal{R}(\bar{\rho}, \mathbf{J}, \alpha_R) + \mathcal{N}\mathcal{A}(\bar{\rho}, \mathbf{J}, \alpha_A)]/2$ is the effective diffusivity, we find that $\dot{\rho}(\mathbf{k}) = -\frac{d\mathcal{T}(\mathbf{k})}{d\rho(\mathbf{k})} \rho(\mathbf{k}) + \eta(\mathbf{k})$ to within first order. This allows us to predict the mean amplitude of fluctuations:

$$\langle \rho(\mathbf{k})^2 \rangle \approx D \left(\left. \frac{\partial \mathcal{T}}{\partial \rho} \right|_{\mathbf{J}, \vec{\alpha}} + \left. \frac{\partial \mathcal{T}}{\partial \mathbf{J}_z} \right|_{\rho, \vec{\alpha}} \frac{\partial \kappa}{\partial \rho} \frac{\mathbf{k}_x^2}{|\mathbf{k}|^2} \right)^{-1}$$

We note that this is independent of the magnitude of \mathbf{k} , and is a function of its direction alone (Fig. 3 a), because of the dipole-like interactions between particles which inhibit current upstream and downstream, while increasing it laterally.

Wall Phase Separation If we assume translation symmetry in the \hat{x} direction $\mathbf{J}(x, z)$ is constant throughout the system. In the discrete model the current through any vertex is proportional to \mathbf{J} , so that we may make the simplification $\mathcal{R}(\rho, \mathbf{J}, \alpha_R) \rightarrow \mathcal{R}(\rho, \alpha_R) \mathbf{J}^{-\alpha_R}$, $\mathcal{A}(\rho, \mathbf{J}, \alpha_A) \rightarrow \mathcal{A}(\rho, \alpha_A) \mathbf{J}^{\alpha_A}$ [31].

We can view a horizontal slice containing A vertices as having uniform density, obeying the dynamics shown in Fig. 3, with a mean addition rate $\mathcal{A}(\rho, \alpha_A)\mathbf{J}^{\alpha_A}\mathcal{N}$, and a mean removal rate of $\mathcal{R}(\rho, \alpha_R)\mathbf{J}^{-\alpha_R}$. The first criteria for a phase separation to occur is mass balance between two horizontal slices of densities ρ_1, ρ_2 :

$$\mathcal{N} = \frac{\mathcal{R}(\rho_1, \alpha_R)\mathbf{J}^{-\alpha_R}}{\mathcal{A}(\rho_1, \alpha_A)\mathbf{J}^{\alpha_A}} = \frac{\mathcal{R}(\rho_2, \alpha_R)\mathbf{J}^{-\alpha_R}}{\mathcal{A}(\rho_2, \alpha_A)\mathbf{J}^{\alpha_A}} = \tilde{\mathcal{N}}\frac{\mathbf{J}^{-\alpha_R}}{\mathbf{J}^{\alpha_A}} \quad (4)$$

where we have defined $\tilde{\mathcal{N}}$ in order to separate the dependence of \mathbf{J} and ρ . Assuming each slice is large ($A \rightarrow \infty$), we may find a recursion relation for the equilibrium distribution of densities:

$$\frac{P(\rho + 1/A)}{P(\rho)} \approx \frac{\mathcal{A}(\rho', \alpha_A)\tilde{\mathcal{N}}}{\mathcal{R}(\rho', \alpha_R)},$$

giving conditions for free energy balance:

$$\int_{\rho_1}^{\rho_2} \ln \left[\frac{\mathcal{A}(\rho', \alpha_A)\tilde{\mathcal{N}}}{\mathcal{R}(\rho', \alpha_R)} \right] d\rho' = 0. \quad (5)$$

The continuum model predicts the system to form walls when $\bar{\rho}$ falls between a satisfying ρ_1, ρ_2 . Note that the wall phase separation is independent of \mathbf{J} .

Channelization Phase Separation If we assume translation symmetry in the \hat{z} direction, the mean current does not have to be uniform; $\mathbf{J}(x, z) = \kappa(\rho(x))\hat{z}$. As before, each *vertical* slice will obey the dynamics in Fig. 3, except the mean removal rate is now $\mathcal{R}(\rho, \alpha_R)\kappa(\rho)^{-\alpha_R}$, while the mean addition rate becomes $\mathcal{N}\mathcal{A}(\rho, \alpha_A)\kappa(\rho)^{\alpha_A}$. Following the same procedure (see appendix for details), the criteria for mass balance becomes:

$$\mathcal{N} = \frac{\mathcal{R}(\rho_1, \alpha_R) \kappa(\rho_1)^{-\alpha_R}}{\mathcal{A}(\rho_1, \alpha_A) \kappa(\rho_1)^{\alpha_A}} = \frac{\mathcal{R}(\rho_2, \alpha_R) \kappa(\rho_2)^{-\alpha_R}}{\mathcal{A}(\rho_2, \alpha_A) \kappa(\rho_2)^{\alpha_A}}$$

and the condition for free energy balance becomes

$$\int_{\rho_1}^{\rho_2} \ln \left[\frac{\mathcal{A}(\rho', \alpha_A)\mathcal{N}\kappa(\rho')^{\alpha_A + \alpha_R}}{\mathcal{R}(\rho', \alpha_R)} \right] d\rho' = 0.$$

Note that when $\alpha_A = -\alpha_R$, the criteria for wall-building and channelization become identical; if a phase separation occurs, it will occur in both orientations, giving rise to a clumping phase transition. This is what we have observed in simulations.

Our continuum model predicts the formation of walls, channels and clumps. However, the functions characterizing conductivity and activity used in this continuum model come from numerical experiments which neglect microscopic correlations, resulting in an incorrect prediction of the order of the phase transition. In addition, because there is no inherent length scale to the continuum model, it can not explain the transition between thin and thick structures. A continuum model considering the formation of the thinnest structures also predicts channelization and walling (Append. D), but a theory combining both elements has no additional predictive power. Additionally the model predicts scale-free dipole-like correlations observed in the discrete model, which ought to exist in all nearly-disordered systems with these properties.

Discussion: Our model relies on very simple elements found across multiple living and nonliving systems; indeed, a coarse-grained view would often yield the same model of a stochastically evolving porous medium where the resistance and flow are coupled to each other, in the presence of a conserved current. Despite this simplicity, our discrete numerical simulations show channeling and walling phase separations at multiple length scales and orientations consistent with the biases of systems it is inspired by. However, whether or not the entire phase diagram of possible configurations is explored in natural systems remains unknown.

Acknowledgments: We thank Mehran Kardar for discussions about the nature and order of the phase transitions, and suggesting the short length scale mean-field theory. For partial financial support, we thank the Henry W. Kendall physics fellowship (S.O), the Wyss Institute and the MacArthur Foundation (L.M) and Human Frontiers Science Program grant RGP0066/2012-TURNER(S.O., L.M.).

[1] N. Schorghofer, B. Jensen, A. Kudrolli, and D. H. Rothman, *Journal of Fluid Mechanics* **503**, 357 (2004).
 [2] A. Mahadevan, A. Orpe, A. Kudrolli, and L. Mahadevan, *EPL (Europhysics Letters)* **98**, 58003 (2012).
 [3] P. Duxbury, P. Leath, and P. Beale, *Physical Review B* **36**, 367 (1987).
 [4] S. Zapperi, P. Ray, H. E. Stanley, and A. Vespignani, *Physical Review Letters* **78**, 1408 (1997).
 [5] A. Tero, S. Takagi, T. Saigusa, K. Ito, D. P. Bebbler,

M. D. Fricker, K. Yumiki, R. Kobayashi, and T. Nakagaki, *Science* **327**, 439 (2010).
 [6] K. Alim, G. Amselem, F. Peaudecerf, M. P. Brenner, and A. Pringle, *Proceedings of the National Academy of Sciences* **110**, 13306 (2013).
 [7] T. Nakagaki and R. D. Guy, *Soft Matter* **4**, 57 (2008).
 [8] L. L. M. Heaton, E. López, P. K. Maini, M. D. Fricker, and N. S. Jones, *Proceedings of the Royal Society B: Biological Sciences* (2010).

- [9] L. Heaton, B. Obara, V. Grau, N. Jones, T. Nakagaki, L. Boddy, and M. D. Fricker, *Fungal Biology Reviews* **26**, 12 (2012).
- [10] A. R. Pries, A. J. M. Cornelissen, A. A. Sloot, M. Hinkeldey, M. R. Dreher, M. Höpfner, M. W. Dewhirst, and T. W. Secomb, *PLoS Comput Biol* **5**, e1000394 (2009).
- [11] T. Masumura, K. Yamamoto, N. Shimizu, S. Obi, and J. Ando, *Arteriosclerosis, Thrombosis, and Vascular Biology* (2009).
- [12] J. W. Song and L. L. Munn, *Proceedings of the National Academy of Sciences* **108**, 15342 (2011).
- [13] F. le Noble, V. Fleury, A. Pries, P. Corvol, A. Eichmann, and R. S. Reneman, *Cardiovascular Research* **65**, 619 (2005).
- [14] D. Szczerba and G. Székely, *Journal of Theoretical Biology* **234**, 87 (2005).
- [15] A. Kamiya, R. Bukhari, and T. Togawa, *Bulletin of mathematical biology* **46**, 127 (1984).
- [16] J. S. Turner, *Cimbebasia* **16**, 143 (2000).
- [17] P. T. Starks and D. C. Gilley, *Naturwissenschaften* **86**, 438 (1999).
- [18] J. S. Turner, *Swarm Intelligence* **5**, 19 (2010).
- [19] B. Heinrich, *Journal of Experimental Biology* **91**, 25 (1981).
- [20] C. Jost, J. Verret, E. Casellas, J. Gautrais, M. Challet, J. Lluc, S. Blanco, M. J. Clifton, and G. Theraulaz, *Journal of the Royal Society Interface* **4**, 107 (2007).
- [21] P. Howse, *Nature* **210**, 967 (1966).
- [22] This particular expression for v chosen for rotational invariance.
- [23] D. T. Gillespie, *Annual Review of Physical Chemistry* **58**, 35 (2007).
- [24] A related model involving local movement gives very similar behavior (Append. B).
- [25] K.-t. Leung, B. Schmittmann, and R. K. P. Zia, *Phys. Rev. Lett.* **62**, 1772 (1989).
- [26] B. Schmittmann and R. K. P. Zia, *Physics reports* **301**, 45 (1998).
- [27] We are limited to small system sizes, and thus a short-ranged local density function, for computational reasons. See Appendix. A for details of determining bimodality.
- [28] A complete continuum model should involve spatial terms to account for a short wavelength cutoff; here we do not include terms in \mathcal{A} , \mathcal{R} , κ that involve spatial derivatives, focusing on the homogeneous mean field limit.
- [29] Making analytical approximations gives similar qualitative behavior, although the agreement with simulations is not as good (Append. C).
- [30] While our continuum model is a non-equilibrium system with no detailed balance, when certain limits and symmetries are assumed.
- [31] This is because in any region $v \propto \mathbf{J}$, and therefore $r(v) \propto v^{-\alpha_R} \propto \mathbf{J}^{-\alpha_R}$, $a(v) \propto v^{\alpha_A} \propto \mathbf{J}^{\alpha_A}$.
- [32] G. Guennebaud, B. Jacob, *et al.*, “Eigen v3,” <http://eigen.tuxfamily.org> (2010).

Appendix A: Determining if a histogram is bimodal

Each simulation i at a particular parameter value gives us a $P_i(N)$, the probability of measuring a N particles in a row, column, or clump in simulation. Averaging many individual simulations allows us to calculate an average $P(N)$, as well as $\sigma(N)$, the estimated standard deviation of this average measurement. We use a 3-sigma threshold of statistical significance—we are significantly more likely to measure N particles than N' iff

$$P(N) - P(N') > 3\sqrt{\sigma(N)^2 + \sigma(N')^2} \quad (\text{A1})$$

If a local maximum $P(N)$ can reach a larger $P(N'')$ without moving through a valley where (A1) holds, it is considered to be a *false peak*. If not, it is considered to be a *true peak*. A histogram with at least two true peaks is considered to be bimodal.

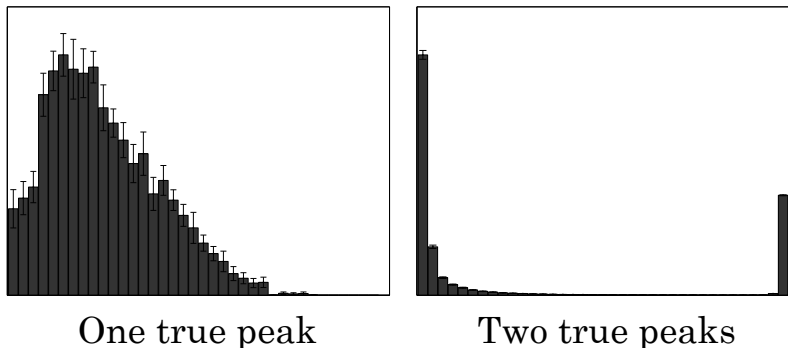


FIG. 4 The distribution on the left has many false peaks, but is not considered to be bimodal. The right distribution is.

Appendix B: Comparison to local dynamics

For local dynamics, we use a slightly modified time integration step.

1. Remove a particle from filled vertex i randomly selected with probability proportional to $r(v_i)$.
2. Solve for the new current through the network.
3. Add the particle to an empty vertex j randomly selected with probability proportional to $a(v_j) e^{-\frac{(r_j - r_i)^2}{2\sigma^2}}$.
4. Solve for the new current through the network.

This prohibits a removed particle from traveling non-locally.

The phase diagram generated is very similar (Fig. 5).

Appendix C: Analytical Mean Field Theory

An alternate mean field theory produces some of the same qualitative behavior. Instead of relying on numerics to find the values of $\mathcal{A}(\rho, \alpha_A)$, $\mathcal{R}(\rho, \alpha_R)$, $\kappa(\rho)$, we rely on a very simple model which gives analytical results.

Channels: For predicting a channelization phase transition, we assume that current is unable to travel in the \hat{x} direction (Fig. 6). Therefore, the equation for conductivity is:

$$\kappa_{\text{chan}}(\rho) = \frac{1}{1 + \Delta\Omega\rho}$$

Because current cannot flow laterally, an equal current of \mathbf{J} is pushed through the filled and empty vertices, and so

$$\mathcal{A}_{\text{chan}}(\rho, \alpha_A) = (1 - \rho), \quad \mathcal{R}_{\text{chan}}(\rho, \alpha_R) = \rho.$$

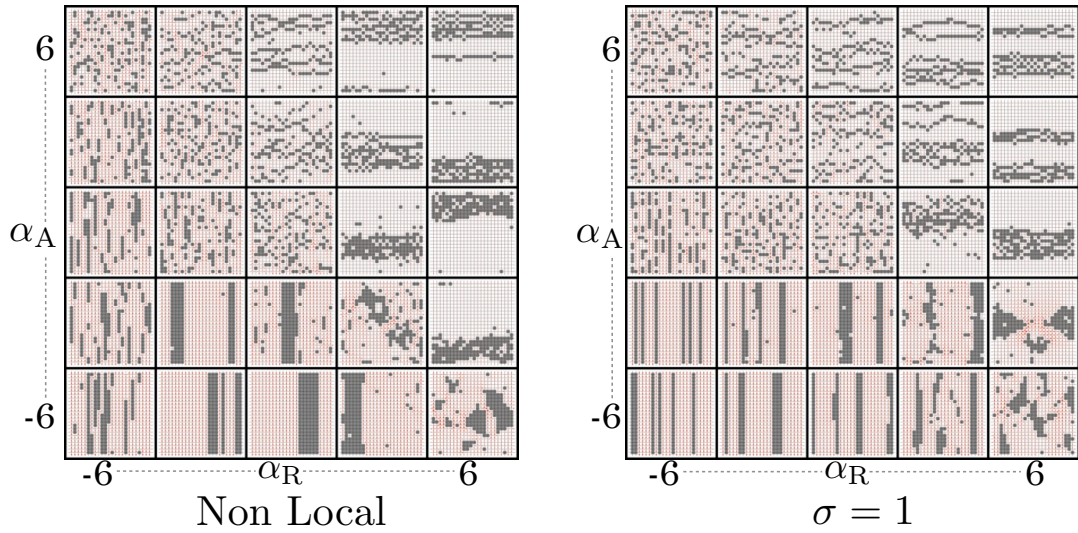
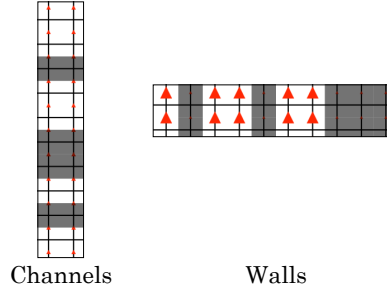


FIG. 5 Comparison of Nonlocal and Local Dynamics

FIG. 6 Schematic of approximations made to obtain analytic forms for \mathcal{A} , \mathcal{R} , κ for channelization and wall-building

We note that $\frac{\mathcal{A}_{\text{wall}} \kappa_{\text{wall}}^{\alpha_A}}{\mathcal{R}_{\text{wall}} \kappa_{\text{wall}}^{-\alpha_R}}$ is a function of $\alpha_A + \alpha_R$, and has no individual dependence on α_A, α_R .

Walls: For predicting a wall phase transition, we assume that, between rows, current can freely flow in the \hat{x} direction without any resistance (Fig. 6). Therefore, the equation for conductivity is

$$\kappa_{\text{wall}}(\rho) = (1 - \rho) + \frac{\rho}{1 + \Delta\Omega}.$$

The total driving across a wall is $\frac{\mathbf{J}}{\kappa_{\text{wall}}}$, and thus the current across an empty vertex is $\frac{\mathbf{J}}{\kappa_{\text{wall}}}$. The total current across a filled vertex is $\frac{\mathbf{J}}{\kappa_{\text{wall}}(1 + \Delta\Omega)}$. Therefore:

$$\mathcal{A}_{\text{wall}}(\rho, \alpha_A) = (1 - \rho) \left(\frac{1}{\kappa_{\text{wall}}(\rho)} \right)^{-\alpha_R}, \quad \mathcal{R}_{\text{wall}}(\rho, \alpha_R) = \rho \left(\frac{1}{\kappa_{\text{wall}}(\rho) (1 + \Delta\Omega)} \right)^{\alpha_A}.$$

We note that $\frac{\mathcal{A}_{\text{wall}}}{\mathcal{R}_{\text{wall}}}$ is also function of $\alpha_A + \alpha_R$, and has no individual dependence on α_A, α_R .

When $\bar{\rho} = .25$, a channelization phase transition occurs when $\alpha_A + \alpha_R \lesssim -1.55$. A wall-building phase transition occurs when $\alpha_A + \alpha_R \gtrsim 2.25$.

Appendix D: Short Length Scale Continuum Model

We can also create a continuum model on a short length scale. To do so, we select a periodic structure with two regions labeled 1 and 2. Region 1 comprises a fraction \mathcal{V}_1 of the squares, while region 2 comprises a fraction \mathcal{V}_2 of squares.

The density will originally be uniform, s.t. $\bar{\rho}_1 = \bar{\rho}_2 = \bar{\rho}$, and a mean density of \mathfrak{s} (Fig. 7) can transfer between squares such that

$$\bar{\rho}_1 = \bar{\rho} + \mathfrak{s}/\mathcal{V}_1, \quad \bar{\rho}_2 = \bar{\rho} - \mathfrak{s}/\mathcal{V}_2$$

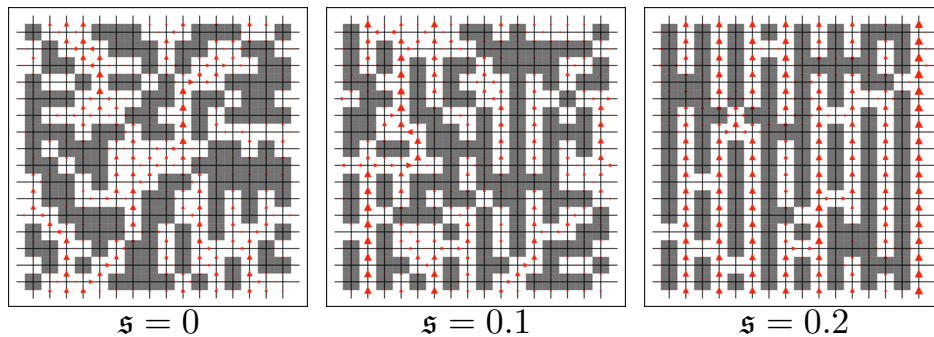


FIG. 7 Example systems where $\bar{\rho} = .5$, $\mathfrak{s} = 0, 0.1, 0.2$, with a spacing of $d = 2$. Orientation is set to channels/pillars.

At a particular imbalance \mathfrak{s} , the probability of an particle moving from region 2 to region 1 divided by the probability of the opposite process gives us a “fugacity”:

$$\mathcal{N}(\bar{\rho}, \mathfrak{s}, \alpha_A, \alpha_R) = \frac{\mathcal{R}_2(\bar{\rho}_2, \kappa(\bar{\rho}, \mathfrak{s}), \alpha_R) \cdot \mathcal{A}_1(\bar{\rho}_1, \kappa(\bar{\rho}, \mathfrak{s}), \alpha_A)}{\mathcal{R}_1(\bar{\rho}_1, \kappa(\bar{\rho}, \mathfrak{s}), \alpha_R) \cdot \mathcal{A}_2(\bar{\rho}_2, \kappa(\bar{\rho}, \mathfrak{s}), \alpha_A)}$$

Therefore, the free energy of a state with an imbalance \mathfrak{s} is

$$- \int_0^{\mathfrak{s}} \text{Ln}[\mathcal{N}(\bar{\rho}, \mathfrak{s}', \alpha_A, \alpha_R)] d\mathfrak{s}'$$

\mathfrak{s} will be set to minimize free energy, and when the optimal \mathfrak{s} is nonzero, the continuum model predicts the system to spontaneously “crystallize” into a form where regions 1 and 2 have different density. For thin channels, region 1 is set by $\delta_{x \bmod d}$, where d some integer which sets the spacing between channels or pillars. This walls are the same except that region 1 is now set by $\delta_{y \bmod d}$.

The short-length scale continuum model gives similar behavior to the uniform continuum model, although the change in free energy is nearly always lower.

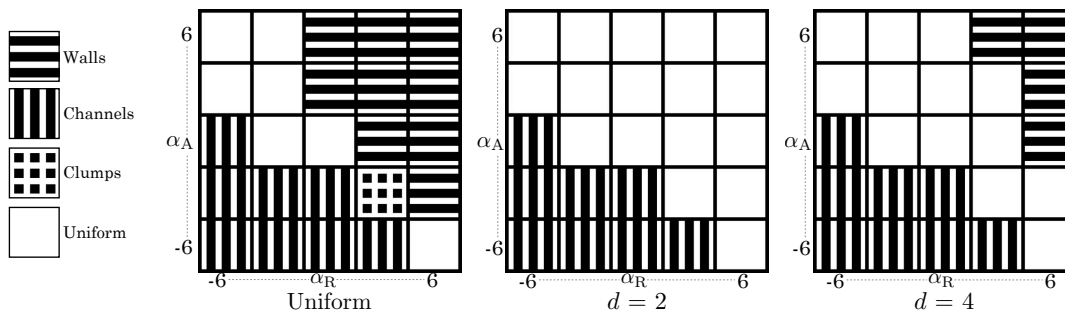


FIG. 8 Comparison of large and small length scale continuum model where $\bar{\rho} = .25$

Appendix E: Low α limit

We start off from a Langevin equation,

$$\dot{\rho} = -\mathcal{T}(\rho, \mathbf{J}(\rho), \vec{\alpha}) + \eta, \quad (\text{E1})$$

Where \mathcal{T} is the time derivative functional, $\vec{\alpha}$ is short for $(\alpha_R, \alpha_A) =$ and \mathbf{J} is itself a functional of ρ obtained by solving (2). We decompose this:

$$\frac{d\mathcal{T}}{d\rho} = \left. \frac{\partial \mathcal{T}}{\partial \rho} \right|_{\mathbf{J}, \vec{\alpha}} + \left. \frac{\partial \mathcal{T}}{\partial \mathbf{J}_z} \right|_{\rho, \vec{\alpha}} \frac{\partial \mathbf{J}_z}{\partial \rho} \quad \left. \frac{\partial \mathcal{T}}{\partial \mathbf{J}_x} \right|_{\rho, \vec{\alpha}} \frac{\partial \mathbf{J}_x}{\partial \rho}$$

We note that, due to symmetry, the third term is zero and may be removed. Moving into fourier space, where $\rho = \rho_0 + \iint \rho(\mathbf{k})e^{i\mathbf{k}\cdot\mathbf{r}}$, we we have:

$$\frac{d\mathcal{T}(\mathbf{k})}{d\rho(\mathbf{k})} = \left. \frac{\partial \mathcal{T}}{\partial \rho} \right|_{\mathbf{J}, \vec{\alpha}} + \left. \frac{\partial \mathbf{J}_z(\mathbf{k})}{\partial \rho(\mathbf{k})} \right|_{\rho, \vec{\alpha}} \frac{\partial \mathbf{J}_z}{\partial \rho}.$$

We now must find:

$$\frac{d\mathbf{J}_z(\mathbf{k})}{d\rho(\mathbf{k})}.$$

To do so, we start off with a uniform density ρ_0 and then apply a sinusoidal perturbation $\Delta\rho e^{i\mathbf{k}\cdot\mathbf{r}}$. The conductivity is, to within first order

$$\kappa = \kappa_0 + \frac{d\kappa}{d\rho} \Delta\rho e^{i\mathbf{k}\cdot\mathbf{r}} = \kappa_0 + \Delta\kappa e^{i\mathbf{k}\cdot\mathbf{r}}$$

Giving us a mean current

$$\mathbf{J} = [\kappa_0 + \Delta\kappa e^{i\mathbf{k}\cdot\mathbf{r}}] \hat{z} - \kappa_0 \nabla [\Delta V e^{i\mathbf{k}\cdot\mathbf{r}}] = \kappa_0 \hat{z} + \Delta\kappa \hat{z} = \mathbf{J}_0 + \Delta\mathbf{J} e^{i\mathbf{k}\cdot\mathbf{r}}, \quad \Delta\mathbf{J} = e^{i\mathbf{k}\cdot\mathbf{r}} [\Delta\kappa \hat{z} - \kappa_0 \nabla [ik_x \hat{x} + ik_z \hat{z}]]$$

We set ΔV to conserve current up to first order:

$$\nabla \cdot \Delta\mathbf{J} = e^{i\mathbf{k}\cdot\mathbf{r}} [\Delta\kappa ik_z + \kappa_0 \Delta V [k_x^2 + k_z^2]] = 0 \Rightarrow \Delta V = \frac{-ik_z}{|k^2| \kappa_0}.$$

Giving us our change in current,

$$\Delta\mathbf{J} = \Delta\rho \frac{d\kappa}{d\rho} \left[\hat{z} + \frac{ik_z}{|k|^2} [ik_x \hat{x} + ik_z \hat{z}] \right] = \Delta\rho \frac{d\kappa}{d\rho} \left[\frac{k_x^2}{|k|^2} \hat{z} - \frac{k_x k_y}{|k|^2} \hat{x} \right] \Rightarrow \frac{d\mathbf{J}_z(\mathbf{k})}{d\rho(\mathbf{k})} = \frac{d\kappa}{d\rho} \frac{\mathbf{k}_x^2}{|\mathbf{k}|^2}, \quad (\text{E2})$$

Plugging E2 into E1 yields:

$$\dot{\rho}(\mathbf{k}) = - \left(\left. \frac{\partial \mathcal{T}}{\partial \rho} \right|_{\mathbf{J}, \vec{\alpha}} + \left. \frac{\partial \mathbf{J}_z}{\partial \rho} \right|_{\rho, \vec{\alpha}} \frac{\partial \kappa}{\partial \rho} \frac{\mathbf{k}_x^2}{|\mathbf{k}|^2} \right) \rho(\mathbf{k}) + \eta(\mathbf{k})$$

where $\langle \eta(\mathbf{k}, t) \eta^*(\mathbf{k}, t') \rangle = 2\delta(t - t')D$. The Einstein relation then predicts the strength of fluctuations to within first order:

$$\langle \rho(\mathbf{k})^2 \rangle \approx D \left(\left. \frac{\partial \mathcal{T}}{\partial \rho} \right|_{\mathbf{J}, \vec{\alpha}} + \left. \frac{\partial \mathbf{J}_z}{\partial \rho} \right|_{\rho, \vec{\alpha}} \frac{\partial \kappa}{\partial \rho} \frac{\mathbf{k}_x^2}{|\mathbf{k}|^2} \right)^{-1}.$$

Appendix F: Higher Order Terms

To find higher order dependencies of \mathcal{T} of $\Delta\rho$, we go through the following steps:

1. Obtain $\Delta\kappa$ from $\Delta\rho$ up to the desired order.
2. Obtain V setting flow to be conserved up to the desired order, e.g. $\nabla \cdot \mathbf{J} = \nabla \cdot [\kappa\hat{z} - \kappa\nabla V] = 0$
3. Obtain \mathbf{J} through $\mathbf{J} = \kappa[\hat{z} - \nabla V]$
4. Obtain \mathcal{T} through ρ, \mathbf{J} up to the desired order.

Here, we will carry out all steps to within second order. We do not go higher as the number of terms increases quite rapidly.

1. Finding change in conductivity

We start from

$$\rho = \rho_0 + \Delta\rho = \rho_0 + \sum_{\mathbf{k}} \rho(\mathbf{k}) e^{i\mathbf{k}\cdot\mathbf{r}}$$

First we must find the change in conductivity, which we split into first and second order components: $\kappa = \kappa_0 + \kappa_1 + \kappa_2 + \mathcal{O}(\Delta\rho^3)$

$$\begin{aligned} \kappa &= \kappa_0 + \Delta\kappa = \kappa_0 + \kappa_\rho \Delta\rho + \frac{1}{2} \kappa_{\rho\rho} \Delta\rho^2 + \mathcal{O}(\Delta\rho^3) = \\ &\kappa_0 + \kappa_\rho \sum_{\mathbf{k}} \Delta\rho(\mathbf{k}) e^{i\mathbf{k}\cdot\mathbf{r}} + \frac{1}{2} \kappa_{\rho\rho} \sum_{\mathbf{k}', \mathbf{k}''} \rho(\mathbf{k}') \rho(\mathbf{k}'') e^{i(\mathbf{k}'+\mathbf{k}'')\cdot\mathbf{r}} + \mathcal{O}(\Delta\rho^3). \end{aligned}$$

Giving us the first order and second order change in conductivity κ_1, κ_2 :

$$\kappa_1(\mathbf{k}) = \kappa_\rho \rho(\mathbf{k}) \tag{F1}$$

$$\kappa_2(\mathbf{k}) = \frac{1}{2} \kappa_{\rho\rho} \rho(\mathbf{k}') \rho(\mathbf{k}'') \delta_{\mathbf{k}'+\mathbf{k}'', \mathbf{k}}. \tag{F2}$$

2. Change in voltage

We must now find the change in voltage, which we do by setting current to be conserved.

$$\nabla \cdot \mathbf{J} = \nabla \cdot [\kappa\hat{z} - \kappa\nabla V] = \kappa_z - \kappa\nabla^2 V - \nabla\kappa \cdot \nabla V + \mathcal{O}(\Delta\rho^3) = 0$$

We separate voltage into it's first and second order components V_1, V_2 :

$$\partial_z \kappa_1 - \kappa_0 \nabla^2 V_1 + \partial_z \kappa_2 - \kappa_1 \nabla^2 V_1 - \kappa_0 \nabla^2 V_2 - \nabla\kappa_1 \cdot \nabla V_1 = 0$$

We solve for V_1 by balancing all first-order terms:

$$\nabla^2 V_1 = \sum_{\mathbf{k}} -|\mathbf{k}|^2 V_1(\mathbf{k}) e^{i\mathbf{k}\cdot\mathbf{r}} = \frac{\partial_z \kappa_1}{\kappa_0} = \frac{1}{\kappa_0} \sum_{\mathbf{k}} i k_z \kappa_1(\mathbf{k}) e^{i\mathbf{k}\cdot\mathbf{r}} \tag{F3}$$

$$\Rightarrow V_1(\mathbf{k}) = \frac{-i k_z}{\kappa_0 |\mathbf{k}|^2} \kappa_1(\mathbf{k}). \tag{F4}$$

To calculate voltage to second order, there are four contributions which must be matched;

$$\partial_z \kappa_2 - \kappa_1 \nabla^2 V_1 - \kappa_0 \nabla^2 V_2 - \nabla\kappa_1 \cdot \nabla V_1 = 0$$

Fortunately, there is only one factor of V_2 which we can move to the left hand side:

$$\begin{aligned} \kappa_0 \nabla^2 V_2 &= \partial_z \kappa_2 - \kappa_1 \nabla^2 V_1 - \nabla \kappa_1 \cdot \nabla V_1 \\ \Rightarrow \sum_{\mathbf{k}} \left(-\kappa_0 |\mathbf{k}|^2 \right) V_2(\mathbf{k}) e^{i\mathbf{k}\cdot\mathbf{r}} &= \underbrace{\sum_{\mathbf{k}} i\mathbf{k}_z \kappa_2(\mathbf{k}) e^{i\mathbf{k}\cdot\mathbf{r}}}_{\partial_z \kappa_2} - \sum_{\mathbf{k}', \mathbf{k}''} V_1(\mathbf{k}') \kappa_1(\mathbf{k}'') \left[\underbrace{-|\mathbf{k}'|^2}_{\kappa_1 \nabla^2 V_1} - \underbrace{\mathbf{k}' \cdot \mathbf{k}''}_{\nabla \kappa_1 \cdot \nabla V_1} \right] e^{i(\mathbf{k}'+\mathbf{k}'')\cdot\mathbf{r}} \\ \Rightarrow V_2(\mathbf{k}) &= \left(\kappa_0 |\mathbf{k}|^2 \right)^{-1} \left[-i\mathbf{k}_z \kappa_2(\mathbf{k}) + \frac{i\mathbf{k}'_z}{\kappa_0} \left(\frac{|\mathbf{k}'|^2 + \mathbf{k}' \cdot \mathbf{k}''}{|\mathbf{k}'|^2} \right) \kappa_1(\mathbf{k}') \kappa_1(\mathbf{k}'') \delta_{\mathbf{k}'+\mathbf{k}'', \mathbf{k}} \right] \end{aligned}$$

Which we then simplify using $\mathbf{k} \delta_{\mathbf{k}'+\mathbf{k}'', \mathbf{k}} = (\mathbf{k}' + \mathbf{k}'') \delta_{\mathbf{k}'+\mathbf{k}'', \mathbf{k}}$:

$$\Rightarrow V_2(\mathbf{k}) = \left(\kappa_0 |\mathbf{k}|^2 \right)^{-1} \left[-i\mathbf{k}_z \kappa_2(\mathbf{k}) + \frac{i\mathbf{k}'_z}{\kappa_0} \left(\frac{\mathbf{k}' \cdot \mathbf{k}}{|\mathbf{k}'|^2} \right) \kappa_1(\mathbf{k}') \kappa_1(\mathbf{k}'') \delta_{\mathbf{k}'+\mathbf{k}'', \mathbf{k}} \right]. \quad (\text{F5})$$

3. Change in mean flow

We start off from the equation for \mathbf{J} :

$$\mathbf{J} = \kappa (\hat{z} - \nabla V)$$

Accumulating first and second order terms

$$\mathbf{J} = \kappa_0 \hat{z} + \kappa_1 \hat{z} + \kappa_2 \hat{z} - \kappa_0 \nabla V_1 - \kappa_0 \nabla V_2 - \kappa_1 \nabla V_1 + \mathcal{O}(\Delta \rho^3)$$

We first calculate the first-order current, \mathbf{J}_1 .

$$\begin{aligned} \mathbf{J}_1 &= \kappa_1 \hat{z} - \kappa_0 \nabla V_1 = \sum_{\mathbf{k}} \kappa_1(\mathbf{k}) e^{i\mathbf{k}\cdot\mathbf{r}} \hat{z} - \kappa_0 \sum_{\mathbf{k}} \kappa_1(\mathbf{k}) i(\mathbf{k}_x \hat{x} + \mathbf{k}_z \hat{z}) \frac{-ik_z}{\kappa_0 |\mathbf{k}|^2} \mathbf{k}_z = \sum_{\mathbf{k}} \kappa_1(\mathbf{k}) e^{i\mathbf{k}\cdot\mathbf{r}} \left[\hat{z} \frac{\mathbf{k}_x^2}{|\mathbf{k}|^2} - \hat{x} \frac{\mathbf{k}_x \mathbf{k}_z}{|\mathbf{k}|^2} \right] \\ \Rightarrow \mathbf{J}_1(\mathbf{k}) &= \kappa_1(\mathbf{k}) \left[\hat{z} \frac{\mathbf{k}_x^2}{|\mathbf{k}|^2} - \hat{x} \frac{\mathbf{k}_x \mathbf{k}_z}{|\mathbf{k}|^2} \right]. \quad (\text{F6}) \end{aligned}$$

Calculating the second-order current \mathbf{J}_2 , we find:

$$\mathbf{J}_2 = \sum_{\mathbf{k}} \mathbf{J}_2(\mathbf{k}) e^{i\mathbf{k}\cdot\mathbf{r}} = \kappa_2 \hat{z} - \kappa_1 \nabla V_1 - \kappa_0 \nabla V_2$$

We expand this as:

$$\sum_{\mathbf{k}} \mathbf{J}_2(\mathbf{k}) e^{i\mathbf{k}\cdot\mathbf{r}} = \sum_{\mathbf{k}} \kappa_2 \hat{z} - \sum_{\mathbf{k}', \mathbf{k}''} V_1(\mathbf{k}') \kappa_1(\mathbf{k}'') i\mathbf{k}' e^{i(\mathbf{k}'+\mathbf{k}'')\cdot\mathbf{r}} - \sum_{\mathbf{k}} V_2(\mathbf{k}) \kappa_0 i\mathbf{k} e^{i\mathbf{k}\cdot\mathbf{r}}$$

$$\mathbf{J}_2(\mathbf{k}) = \kappa_2 \hat{z} - V_1(\mathbf{k}') \kappa_1(\mathbf{k}'') i\mathbf{k}' \delta_{\mathbf{k}'+\mathbf{k}'', \mathbf{k}} - i\kappa_0 \mathbf{k} V_2(\mathbf{k})$$

Plugging in V_1, V_2 gives us:

$$\mathbf{J}_2(\mathbf{k}) = \kappa_2 \hat{z} - \frac{-i\mathbf{k}'_z}{\kappa_0 |\mathbf{k}'|^2} \kappa_1(\mathbf{k}') \kappa_1(\mathbf{k}'') i\mathbf{k}' \delta_{\mathbf{k}'+\mathbf{k}'', \mathbf{k}}$$

$$-i\kappa_0 \mathbf{k} \left((\kappa_0 |\mathbf{k}|^2)^{-1} \left[-i\mathbf{k}_z \kappa_2(\mathbf{k}) + \frac{i\mathbf{k}'_z}{\kappa_0} \left(\frac{\mathbf{k}' \cdot \mathbf{k}}{|\mathbf{k}'|^2} \right) \kappa_1(\mathbf{k}') \kappa_1(\mathbf{k}'') \delta_{\mathbf{k}'+\mathbf{k}'', \mathbf{k}} \right] \right)$$

We simplify this as:

$$\mathbf{J}_2(\mathbf{k}) = \kappa_2(\mathbf{k}) \left[\hat{z} \frac{\mathbf{k}_x^2}{|\mathbf{k}|^2} - \hat{x} \frac{\mathbf{k}_x \mathbf{k}_z}{|\mathbf{k}|^2} \right] + \frac{\kappa_1(\mathbf{k}') \kappa_1(\mathbf{k}'') \delta_{\mathbf{k}'+\mathbf{k}'', \mathbf{k}}}{\kappa_0} \left[\mathbf{k}'_z \frac{-\mathbf{k}' |\mathbf{k}|^2 + \mathbf{k} (\mathbf{k}' \cdot \mathbf{k})}{|\mathbf{k}|^2 |\mathbf{k}'|^2} \right]. \quad (\text{F7})$$

Here, we can confirm that

$$\nabla \cdot [e^{i\mathbf{k} \cdot \mathbf{r}} \mathbf{J}_2(\mathbf{k})] = i e^{i\mathbf{k} \cdot \mathbf{r}} [\mathbf{k} \cdot \mathbf{J}_2(\mathbf{k})] = 0.$$

It will be convenient to have this answer divided into x and z components:

$$\mathbf{J}_2(\mathbf{k}) = \kappa_2(\mathbf{k}) \left[\hat{z} \frac{\mathbf{k}_x^2}{|\mathbf{k}|^2} - \hat{x} \frac{\mathbf{k}_x \mathbf{k}_z}{|\mathbf{k}|^2} \right] + \quad (\text{F8})$$

$$\frac{\kappa_1(\mathbf{k}') \kappa_1(\mathbf{k}'') \delta_{\mathbf{k}'+\mathbf{k}'', \mathbf{k}}}{\kappa_0} \left[\hat{z} \mathbf{k}'_z \frac{-\mathbf{k}'_z |\mathbf{k}|^2 + \mathbf{k}_z (\mathbf{k}' \cdot \mathbf{k})}{|\mathbf{k}|^2 |\mathbf{k}'|^2} + \hat{x} \mathbf{k}'_z \frac{-\mathbf{k}'_x |\mathbf{k}|^2 + \mathbf{k}_x (\mathbf{k}' \cdot \mathbf{k})}{|\mathbf{k}|^2 |\mathbf{k}'|^2} \right]. \quad (\text{F9})$$

4. Change in \mathcal{T}

Likewise, we may represent the change in the time derivative functional:

$$\mathcal{T}(\rho, \mathbf{J}, \vec{\alpha}) = \mathcal{T}_\rho \Delta \rho + \mathcal{T}_\mathbf{J} \mathbf{J}_1 + \mathcal{T}_\mathbf{J} \mathbf{J}_2 + \frac{1}{2} (\mathcal{T}_{\mathbf{J}\mathbf{J}} \mathbf{J}_1^2 + \mathcal{T}_{\rho\rho} \Delta \rho^2 + 2\mathcal{T}_{\mathbf{J}\rho} \Delta \rho \mathbf{J}_1) + \mathcal{O}(\Delta \rho^3)$$

We note that, due to symmetry, \mathcal{T} is even with respect to \mathbf{J}_x are relevant. Therefore we may simplify the time derivative as:

$$\mathcal{T} = \mathcal{T}_\rho \Delta \rho + \mathcal{T}_{\mathbf{J}_z} \mathbf{J}_{1z} + \mathcal{T}_{\mathbf{J}_z} \mathbf{J}_{2z} + \frac{1}{2} [\mathcal{T}_{\mathbf{J}_z \mathbf{J}_z} \mathbf{J}_{1z}^2 + \mathcal{T}_{\mathbf{J}_x \mathbf{J}_x} \mathbf{J}_{1x}^2 + \mathcal{T}_{\rho\rho} \Delta \rho^2 + 2\mathcal{T}_{\mathbf{J}_z \rho} \mathbf{J}_{1z} \Delta \rho] + \mathcal{O}(\Delta \rho^3),$$

where we have used the notation $\mathbf{J}_{1z} = \mathbf{J}_1 \cdot \hat{z}$, $\mathbf{J}_{1x} = \mathbf{J}_1 \cdot \hat{x}$, $\mathbf{J}_{2z} = \mathbf{J}_2 \cdot \hat{z}$.

We recover the first order component \mathcal{T}_1 as before:

$$\mathcal{T}_1 = \mathcal{T}_\rho \Delta \rho + \mathcal{T}_{\mathbf{J}_z} \mathbf{J}_{1z} \Rightarrow \mathcal{T}_1(\mathbf{k}) = \left[\mathcal{T}_\rho + \mathcal{T}_{\mathbf{J}_z} \kappa_\rho \frac{\mathbf{k}_x^2}{|\mathbf{k}|^2} \right] \rho(\mathbf{k}).$$

We now calculate the second order component \mathcal{T}_2 :

$$\mathcal{T}_2 = \mathcal{T}_{\mathbf{J}_z} \mathbf{J}_{2z} + \frac{1}{2} [\mathcal{T}_{\mathbf{J}_z \mathbf{J}_z} \mathbf{J}_{1z}^2 + \mathcal{T}_{\mathbf{J}_x \mathbf{J}_x} \mathbf{J}_{1x}^2 + \mathcal{T}_{\rho\rho} \Delta \rho^2 + 2\mathcal{T}_{\mathbf{J}_z \rho} \mathbf{J}_{1z} \Delta \rho]$$

Which we may decompose as:

$$\mathcal{T}_2(\mathbf{k}) = \mathcal{T}_{\mathbf{J}_z} \mathbf{J}_{2z} + \frac{1}{2} [\mathcal{T}_{\mathbf{J}_z \mathbf{J}_z} \mathbf{J}_{1z}(\mathbf{k}') \mathbf{J}_{1z}(\mathbf{k}'') + \mathcal{T}_{\mathbf{J}_x \mathbf{J}_x} \mathbf{J}_{1x}(\mathbf{k}') \mathbf{J}_{1x}(\mathbf{k}'') + \mathcal{T}_{\rho\rho} \rho(\mathbf{k}') \rho(\mathbf{k}'') + 2\mathcal{T}_{\mathbf{J}_z \rho} \mathbf{J}_{1z}(\mathbf{k}') \rho(\mathbf{k}'')] \delta_{\mathbf{k}'+\mathbf{k}'', \mathbf{k}}$$

Substituting \mathbf{J}_{1z} , \mathbf{J}_{2z} , \mathbf{J}_{1x} , we get:

$$\mathcal{T}_2(\mathbf{k}) = \mathcal{T}_{\mathbf{J}_z} \left[\frac{1}{2} \kappa_{\rho\rho} \frac{\mathbf{k}_x^2}{|\mathbf{k}|^2} \rho(\mathbf{k}') \rho(\mathbf{k}'') \delta_{\mathbf{k}'+\mathbf{k}'', \mathbf{k}} + \frac{\kappa_1(\mathbf{k}') \kappa_1(\mathbf{k}'') \delta_{\mathbf{k}'+\mathbf{k}'', \mathbf{k}} \mathbf{k}'_z \frac{-\mathbf{k}'_z |\mathbf{k}|^2 + \mathbf{k}_z (\mathbf{k}' \cdot \mathbf{k})}{|\mathbf{k}|^2 |\mathbf{k}'|^2} \right] +$$

$$\frac{1}{2} \left[\mathcal{T}_{\mathbf{J}_z \mathbf{J}_z} \kappa_1(\mathbf{k}') \kappa_1(\mathbf{k}'') \frac{(\mathbf{k}'_x)^2 (\mathbf{k}''_x)^2}{|\mathbf{k}'|^2 |\mathbf{k}''|^2} + \mathcal{T}_{\mathbf{J}_x \mathbf{J}_x} \kappa_1(\mathbf{k}') \kappa_1(\mathbf{k}'') \frac{\mathbf{k}'_x \mathbf{k}'_z \mathbf{k}''_x \mathbf{k}''_z}{|\mathbf{k}'|^2 |\mathbf{k}''|^2} + \mathcal{T}_{\rho\rho} \rho(\mathbf{k}') \rho(\mathbf{k}'') + 2 \mathcal{T}_{\mathbf{J}_z \rho} \kappa_1(\mathbf{k}') \rho(\mathbf{k}'') \frac{(\mathbf{k}'_x)^2}{|\mathbf{k}'|^2} \right] \delta_{\mathbf{k}'+\mathbf{k}'', \mathbf{k}}$$

We shuffle some terms around to get

$$\mathcal{T}_2(\mathbf{k}) = (\rho(\mathbf{k}') \rho(\mathbf{k}'') \delta_{\mathbf{k}'+\mathbf{k}'', \mathbf{k}}) \frac{1}{2} \left[\mathcal{T}_{\rho\rho} + \mathcal{T}_{\mathbf{J}_z} \kappa_{\rho\rho} \frac{\mathbf{k}_x^2}{|\mathbf{k}|^2} \right]$$

$$+ \kappa_1(\mathbf{k}') \kappa_1(\mathbf{k}'') \delta_{\mathbf{k}'+\mathbf{k}'', \mathbf{k}} \left[\frac{\mathcal{T}_{\mathbf{J}_z} \mathbf{k}'_z \frac{-\mathbf{k}'_z |\mathbf{k}|^2 + \mathbf{k}_z (\mathbf{k}' \cdot \mathbf{k})}{|\mathbf{k}|^2 |\mathbf{k}'|^2} + \frac{\mathcal{T}_{\mathbf{J}_z \mathbf{J}_z} \left(\frac{(\mathbf{k}'_x)^2 (\mathbf{k}''_x)^2}{|\mathbf{k}'|^2 |\mathbf{k}''|^2} \right) + \frac{\mathcal{T}_{\mathbf{J}_x \mathbf{J}_x} \left(\frac{\mathbf{k}'_x \mathbf{k}'_z \mathbf{k}''_x \mathbf{k}''_z}{|\mathbf{k}'|^2 |\mathbf{k}''|^2} \right)}{2} \right]$$

$$+ \kappa_1(\mathbf{k}') \rho(\mathbf{k}'') \delta_{\mathbf{k}'+\mathbf{k}'', \mathbf{k}} \mathcal{T}_{\mathbf{J}_z \rho} \frac{(\mathbf{k}'_x)^2}{|\mathbf{k}'|^2}$$

And substitute $\kappa_1(\mathbf{k}) = \rho(\mathbf{k}) \kappa_\rho$:

$$\mathcal{T}_2(\mathbf{k}) = (\rho(\mathbf{k}') \rho(\mathbf{k}'') \delta_{\mathbf{k}'+\mathbf{k}'', \mathbf{k}}) \frac{1}{2} \left[\mathcal{T}_{\rho\rho} + \mathcal{T}_{\mathbf{J}_z} \kappa_{\rho\rho} \frac{\mathbf{k}_x^2}{|\mathbf{k}|^2} \right]$$

$$+ (\rho(\mathbf{k}') \rho(\mathbf{k}'') \delta_{\mathbf{k}'+\mathbf{k}'', \mathbf{k}}) (\kappa_\rho)^2 \left[\frac{\mathcal{T}_{\mathbf{J}_z} \mathbf{k}'_z \frac{-\mathbf{k}'_z |\mathbf{k}|^2 + \mathbf{k}_z (\mathbf{k}' \cdot \mathbf{k})}{|\mathbf{k}|^2 |\mathbf{k}'|^2} + \frac{\mathcal{T}_{\mathbf{J}_z \mathbf{J}_z} \left(\frac{(\mathbf{k}'_x)^2 (\mathbf{k}''_x)^2}{|\mathbf{k}'|^2 |\mathbf{k}''|^2} \right) + \frac{\mathcal{T}_{\mathbf{J}_x \mathbf{J}_x} \left(\frac{\mathbf{k}'_x \mathbf{k}'_z \mathbf{k}''_x \mathbf{k}''_z}{|\mathbf{k}'|^2 |\mathbf{k}''|^2} \right)}{2} \right]$$

$$+ (\rho(\mathbf{k}') \rho(\mathbf{k}'') \delta_{\mathbf{k}'+\mathbf{k}'', \mathbf{k}}) \mathcal{T}_{\mathbf{J}_z \rho} \kappa_\rho \frac{(\mathbf{k}'_x)^2}{|\mathbf{k}'|^2}$$

We obtain our final answer:

$$\mathcal{T}_2(\mathbf{k}) = F(\mathbf{k}, \mathbf{k}', \mathbf{k}'') \rho(\mathbf{k}') \rho(\mathbf{k}'') \delta_{\mathbf{k}'+\mathbf{k}'', \mathbf{k}},$$

Where our interaction function, F , is:

$$F(\mathbf{k}, \mathbf{k}', \mathbf{k}'') = \frac{\mathcal{T}_{\rho\rho}}{2} + \frac{\mathcal{T}_{\mathbf{J}_z} \kappa_{\rho\rho} \frac{\mathbf{k}_x^2}{|\mathbf{k}|^2}}{2} + \frac{\mathcal{T}_{\mathbf{J}_z} (\kappa_\rho)^2 \mathbf{k}'_z \frac{-\mathbf{k}'_z |\mathbf{k}|^2 + \mathbf{k}_z (\mathbf{k}' \cdot \mathbf{k})}{|\mathbf{k}|^2 |\mathbf{k}'|^2}}{\kappa_0}$$

$$+ \frac{\mathcal{T}_{\mathbf{J}_z \mathbf{J}_z} (\kappa_\rho)^2 \left(\frac{(\mathbf{k}'_x)^2 (\mathbf{k}''_x)^2}{|\mathbf{k}'|^2 |\mathbf{k}''|^2} \right) + \frac{\mathcal{T}_{\mathbf{J}_x \mathbf{J}_x} (\kappa_\rho)^2 \left(\frac{\mathbf{k}'_x \mathbf{k}'_z \mathbf{k}''_x \mathbf{k}''_z}{|\mathbf{k}'|^2 |\mathbf{k}''|^2} \right)}{2} + \mathcal{T}_{\mathbf{J}_z \rho} \kappa_\rho \frac{(\mathbf{k}'_x)^2}{|\mathbf{k}'|^2}.$$

We note that $F(\mathbf{k}, \mathbf{k}', \mathbf{k}'') \neq F(\mathbf{k}', \mathbf{k}, \mathbf{k}'')$, and thus can not be written as the derivative of some cubic free energy functional. Therefore, like the discrete model, the continuum model at second order has no detailed balance. This gives a stochastic field equation with no detailed balance and complicated interaction coefficients, and we choose not to proceed further. Note that η will also change with \mathbf{J} , ρ with analogous first-order and second-order terms, but here, we have ignored this extra complexity.

Appendix G: Methods

The code used was written in a combination of C++, MATLAB, and Objective-C, and can be downloaded at <http://web.mit.edu/socko/Public/PublishedCode/ActivePorousMediaCode.zip>. Currents were solved using the Eigen linear equation solver [32].